Calculations of Operational and Residual Doses for the SNS Linac

Franz X. Gallmeier

Oak Ridge National Laboratory
P.O. Box 2008, MS 6474
Oak Ridge, TN 37830
gallmeierfz@ornl.gov

Abstract *–Dose profiles throughout the front-end building and the accelerator tunnel were calculated for the SNS linac system both for normal operation and after shut down of the facility based on normal operations beam losses. The calculated dose levels at an cylindrical envelope with 60 cm radius range from 0.08 to 10 rem/hr for the drift tube linac part, from 50-80 rem/hr for the coupled cavity linac part, from 1 to 20 rem/hr for the superconducting linac part, and from 70-200 rem/hr for the spare section extending after the linac. In the front-end building that houses the first 10 meters of the drift tube linac, dose levels of up to 500 mrem/hr were calculated that need to be reduced by adequate shielding, for example an ordinary concrete shield of up to 120 cm thickness. The shield thickness can be reduced by 25% using borated concrete or a layer of 20 cm borated polyethylene followed by ordinary concrete. The calculated residual dose levels in the accelerator tunnel are a factor of 2000-3000 lower compared to the operational doses assuming a 30-year operations period and a 1hour decay period.*

I. INTRODUCTION

The Spallation Neutron Source (SNS)[1] is powered by a 2-mA, high intensity, 1-GeV proton beam, which is generated in a linac system[2] consisting of a drift tube linac (DTL), a coupled cavity linac (CCL) and a superconducting linac (SCL) and starting out as a H beam. Although the beam losses during normal operation were conceptually minimized, the high beam intensity may cause a radiation hazard. Initially, the design parameter list signed out a generic proton line loss of 1W/m along all the linac beam line as used for earlier analyses[3]. This assumption was thought to coarsely overestimate the anticipated beam losses especially in the first sections of the DTL and in the SCL, so a much more detailed beam loss characteristic was developed based on model calculations and experience gained at existing facilities[4]. Beam loss mechanisms considered include gas stripping, scraping due to halo formation, and beam excursions caused by steering and radio frequency errors in the linac sub-systems. Analyses were performed to study the impact of anticipated proton beam losses in the linac based on this detailed characterization, both for the operation and maintenance periods. As the very first 10 meters of the linac extend into the front-end building, emphasis was laid upon developing a shield around the DTL that lowers the anticipated dose to acceptable levels for maintenance and operations personnel. Overlaid to these dose levels are dark current effects caused by the field gradients in the accelerator structures. These are expected to contribute significantly to the gamma dose, when the RF fields are on even when no beam is delivered. These contributions are not considered in this study.

II. LINAC MODEL FOR THE OPERATIONAL STUDY

Geometric models for the DTL, the CCL and the SCL in the MCNPX[5] input language were developed for earlier studies[3], and were consolidated to one complete linac model.

The linac is assembled from three sections, the DTL, the CCL and the SCL each of which differ significantly in structure from each other. It was decided to prepare MCNPX models for these sections with not only enough

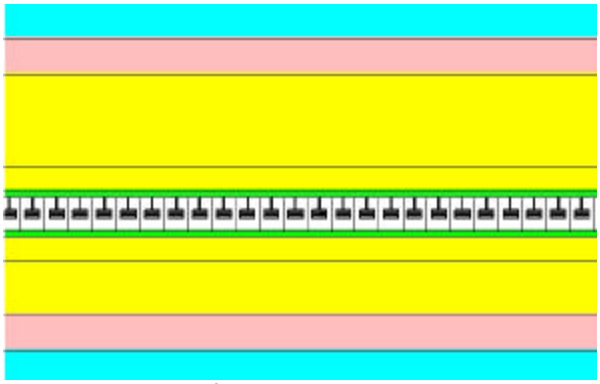

Fig. 1. A section of the MCNPX DTL model showing the drift tubes placed in a DTL tank.

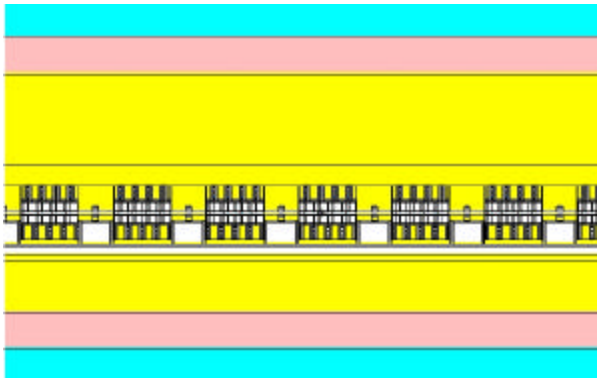

Fig. 2. A section of the CCL model showing the complex cavity structure.

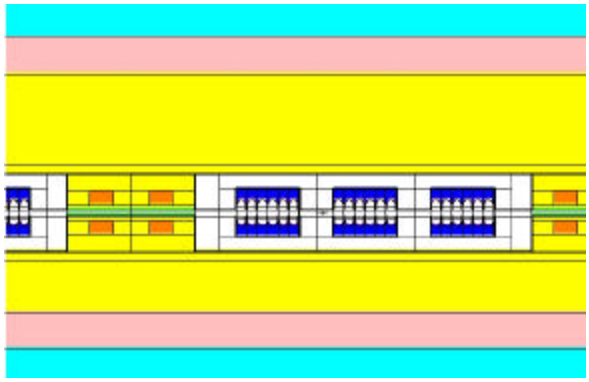

Fig. 3: A low beta SCL module consisting of three helium filled Nb cavities in a vacuum tank.

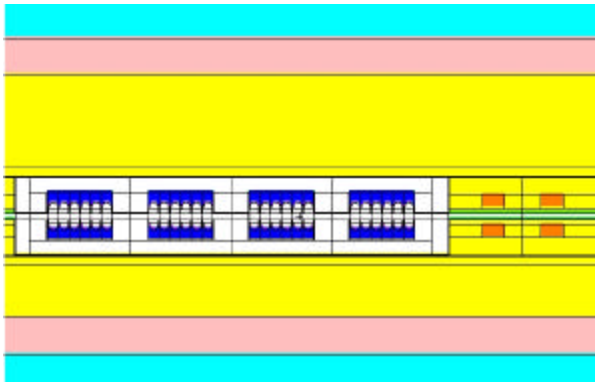

Fig. 4: High beta SCL module consisting of a cryogenic tank and a warm section with beam line magnets.

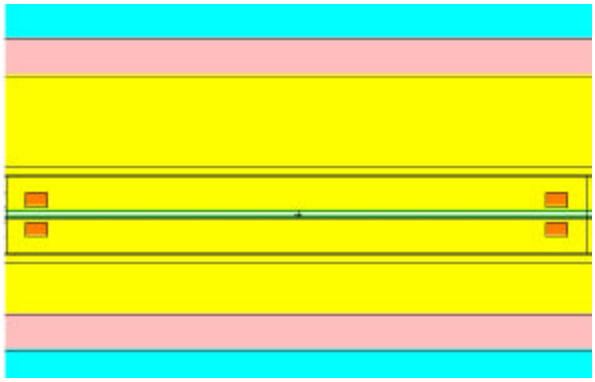

Fig. 5: Spare SCL period for future extensions of the SCL consisting of a warm beam line and steering magnets.

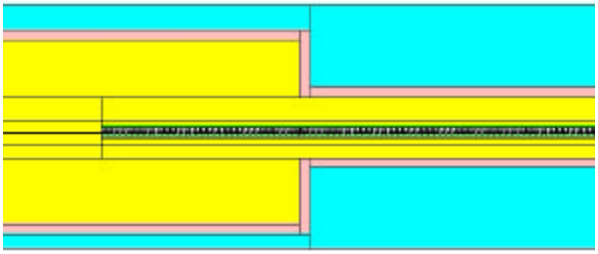

Fig. 6: The front-end building connecting to the linac tunnel and housing the first 10 meters of the DTL.

detail for the shielding analyses, but also enough to perform detailed energy deposition studies later on.

The 37 meter long DTL is modeled as 122 lined up drift tube assemblies of 19 cm length and 11 cm outer diameter consisting of a samarium cobalt magnet in a massive copper casing. The drift tube assemblies hang on copper supply tubes in a carbon steel vacuum tank having a 43 cm inner diameter and 7 cm wall thickness. Fig. 1 shows a cross sectional view of the model.

The CCL is a complex copper structure modeled from 48 segments with lengths of 76 cm that are connected by a beam line and drums of powered coupler units. These segments add up to about 55-meter length of the CCL. A focusing magnet is placed at the center of the connecting beam lines. Each segment consists of a sandwich of square copper plates with about 30 cm base constructing a system of drift tubes and chambers and extending alternating on the top and on the bottom with coupling chambers. Part of the support structure was modeled as two cylindrical steel tubes running parallel to the bottom of the accelerator structure and a vacuum tube between the support structure was included in the model because both added significant mass to the accelerator structures. Fig. 2 presents a sectional view of the model.

Compared to the CCL, the SCL is a very light structure. It consists of 11 medium beta modules, and 12 high beta modules. The modules add up to total lengths of the medium beta and the high beta SCL of 68 and 95 meters, respectively. The SCL modules are connected with "warm" beam lines. A pair of magnets is placed at each of these beam line segments. Each cryomodule was modeled as a voided cylindrical steel tank with a 98 cm inner diameter, 0.6 cm wall thickness closed at both ends with 1.0 cm thick plates. Each medium beta cryomodule contains 3, each high beta cryomodule contains 4 aligned and inter-connected cylindrical helium filled steel vessels with 60 cm outer diameter and 0.2 cm wall thickness. Each helium vessel is penetrated by a voided bellow-like niobium cavity with about a 30 cm outer diameter and 0.4 cm wall thickness as shown in Fig.3 and 4.

The linac extends with a 71-meter long spare section that is intended to hold a future linac extension of 9 additional high beta SCL modules and that would allow proton energies up to 1.3 GeV. A period of this section consists of a steel beam pipe and a set of two steering magnets as shown in Fig. 5.

As much use as possible was made of the lattice features of the MCNPX geometry capabilities to obtain a compact manageable geometry description culminating in a three-layer lattice hierarchy for the SCL. For this reason the drift tube and cavity lengths that continuously increase with the proton energy could not be modeled which was a minor model disadvantage. Also vacuum pumps, supply lines, support structures, and other equipment in the accelerator tunnel, other than that mentioned above, was not considered.

All the linac structure was modeled in the tunnel environment including the 46 cm thick ordinary concrete walls and several meters of soil. The very first 10 meters of the DTL are located in the front-end building, which houses the ion source, the medium energy beam transfer (MEBT) lines and some laboratories, as well as the personnel access point for the linac tunnel. This area was modeled as an air filled cylindrical zone bound by concrete walls attached to the tunnel as shown in Fig. 6.

III. LINAC MODELS FOR THE ACTIVATION STUDIES

Constraints of the transport code system forced us to perform the activation analyses in parts. Also a module of the code system was not able to extract meaningful and detailed information from tracking particles in repeated structures, which were heavily use in building the models. Details about the code limitations will be discussed later. Consequently, much more simplified models were generated for the DTL, CCL, and SCL including the spare section homogenizing detailed structures into large cells. Although the models were simplified, the number of cells that were used was much higher than for the detailed model because each linac period had to be modeled explicitly.

In the DTL model, each of the 6 DTL tanks was modeled separately, with the drift tubes and their supply tubes modeled as homogenized zones (see Fig. 7). The drift tube lengths increasing with particle energy were considered by applying different homogenized mixtures for each tank that reflected the changes in the copper and permanent magnet masses for each tank. The CCL model is compiled of 48 periods, each of which consists of zones with various copper densities reflecting the complex CCL structure (see Fig. 8). A fraction of water was mixed into some zones to account for the cooling water. For the SCL modules, the helium filled vessels containing the niobium cavities are smeared out into two large zones extending throughout the length of a cryomodule (see Fig. 9 and 10).

Fig.7: A 8 meter section of the DTL activation model.

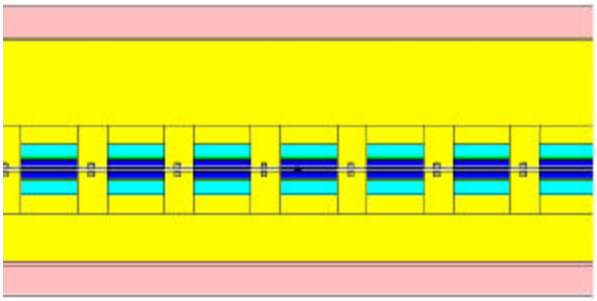

Fig. 8: A 8 meter section of the CCL activation model.

Fig. 9: A 8 meter section of the SCL activation model including a low beta module.

Fig. 10: A 8 meter section of the SCL activation model including a high beta module.

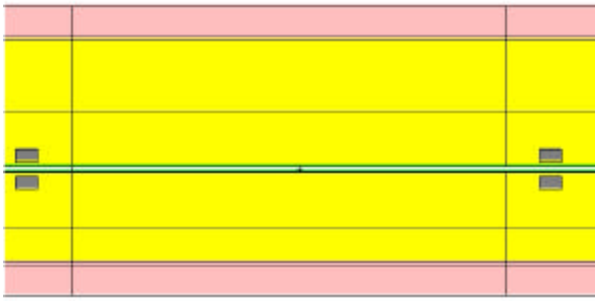

Fig. 11: A 8 meter section of the SCL activation model showing a spare period following the linac.

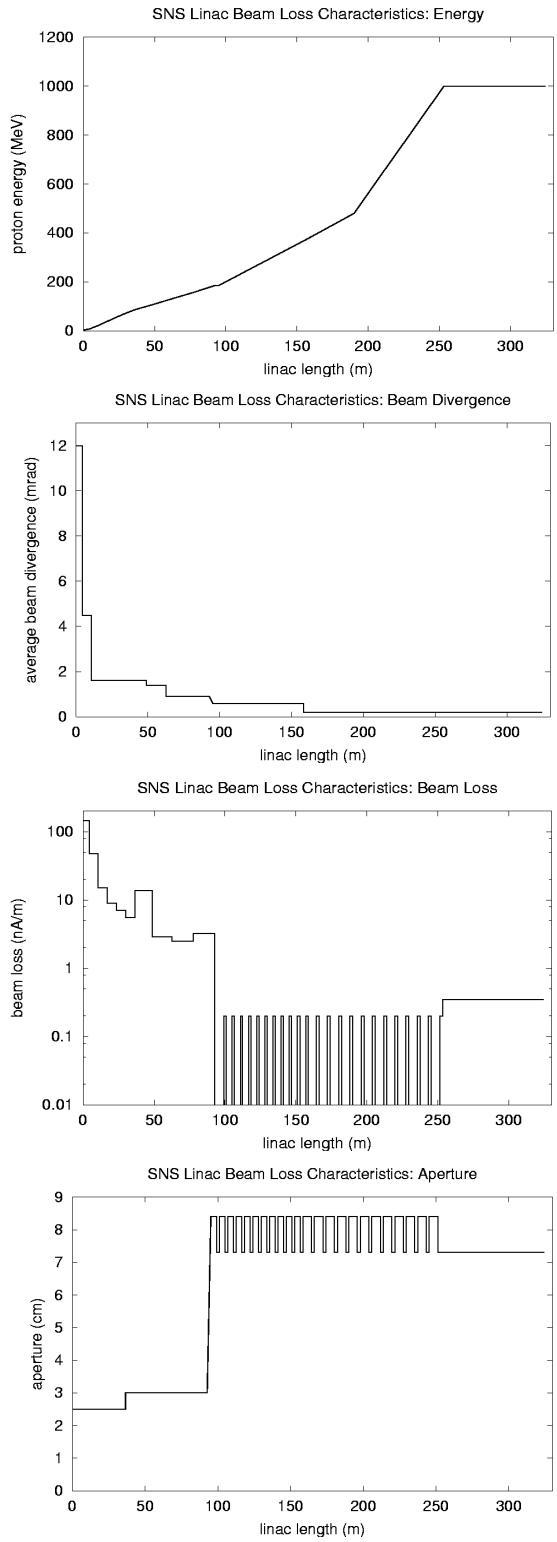

Fig. 12: Characteristica of the anticipated proton beam losses in the SNS linac during normal operation.

IV. METHODOLOGY OF THE CALCULATIONS

The dose levels in the accelerator tunnel were calculated entirely applying the MCNPX[5] Monte Carlo multi particle transport code. The proton beam loss characteristics as shown in Fig. 12 were modeled with the standard MCNPX input cards as defined by the SNS beam loss document[4]. 8 source points were defined around the circumference of the beam aperture at 450 locations along the linac length with energy, position and flight direction adjusted to the definitions. In the SCL section, beam losses are only expected in the warm sections that connect the cryomodules because the warm sections have a smaller aperture compared to the cavities and therefore act as beam scraper.

Surface flux tallies and tracklength tallies were applied to obtain neutron and gamma fluxes. The surface tallies were defined at a cylindrical envelope with 60cm radius around the linac structure and averaged over 50-100 cm long segments. For the SCL section the radius of the envelope was extended to 79 cm to allow to report dose values at 1-foot distance from the accelerator structure as requested. The tracklength tallies sampled over the tunnel air volumes outside of the cylindrical envelope in 50-100 cm long segments. Further tracklength tallies were arranged in the frontend area the air volumes extending to the sides from the tunnel cross-sectional area. Dose results were obtained from the flux results applying flux-to-dose conversion factors taken from the HILO multigroup cross section library[6]. The neutron flux-to-dose conversion factors are defined up to the energy of 400 MeV. For neutrons with energies above this limit the highest energy flux-to-dose conversion factor was used. For the operational cases the detailed model was applied, for the activation cases the simplified models were used.

The thickness of shields required to reduce the dose in the first 10 meters of the DTL was evaluated with a hybrid Monte Carlo and discrete ordinates approach. Events of neutron and gamma leakages saved on a file during the MCNPX calculation were binned energy-wise into the multi-group structure of the HILO cross section library and angle-wise into a symmetric S64 angular quadrature set. This information was converted to a cylindrical shell source with the MTA coupling tool[7], and used in one-dimensional coupled neutron-gamma discrete-ordinates transport analyses applying the ANISN[8] code and the HILO cross section library.

For the activation analyses the Activation Analysis System (AAS)[9] was applied. This system builds on the ORIHET[10] code that is fed with isotopic production rates calculated directly or indirectly with the MCNPX code. The isotope production rates due to high-energy spallation

reactions are taken from history information written by MCNPX and analyzed by the HTAPE code. The neutron activation contribution to the production rates is calculated folding average neutron fluxes with activation cross sections from the FENDL library[11]. So far the HTAPE code is only able to give cell-averaged values of isotopic production rates, the repeated structure features of the MCNPX code are not supported yet. Therefore the geometric part of the linac model had to be completely rewritten for the activation analyses. For the MCNPX calculations a multitasking parallel version of the MCNPX code based on the PVM library was applied running on a 28-node dual processor LINUX cluster providing results in a reasonable time. The bottleneck in the activation analysis sequence was found to be the HTAPE code that has to digest huge history files and is only operational on a serial environment. An activation tally option was implemented into MCNPX that directly samples the production rates in the MCNPX run to circumvent this problem.

All residual dose calculations were again performed using the MCNPX code. The gamma production spectra were extracted from the ORIHET outputs and formatted into source descriptions in the MCNPX input language. The ORIHET is configured to give the decay photon spectra in the multi-group structure of the DABL sand the HILO libraries. MCNPX picks the cell from a probability table reflecting the photon source strengths, and picks the energy from the gamma spectra. The location within the cell is randomly sampled with the rejection technique. The MCNPX general source card allows 999 distribution functions to be used which limited the number of cells with activation sources to be applied in one calculation. For one cell one has to specify the energy distribution, and a radial and axial spacial distributions to be used for sampling the source location with the rejection technique. At least three distribution functions per cell are required meaning that about 300 activation cells can be included into the source. The CCL and SCL models exceeded this limit by a factor of two. Hence the activation calculations have to be performed in pieces with the benefit that the dose contributions from linac structure cells and concrete cells were separated.

V. RESULTS

For the normal operations szenario, the doses outside of the linac structures at 60 cm distance from the beam axis are shown in Fig. 13, the dose averaged over the tunnel air volume is presented in Fig. 14. The dominating contribution to the doses is by the neutrons generated in spallation reactions. The energy differential neutron dose contributions are plotted in Fig. 15 for different locations in the linac together with the neutron flux-to-dose conversion factors. The high-energy neutron cut off reflects the particle energy of the respective linac location. Neurons above 0.1 MeV contribute most of the dose, which is coincident with the high energy plateau of the flux-to-dose conversion factors which is about two orders of magnitude above values in the low-energy range.

The dose at the linac envelope is about a factor of 2 higher compared to the averaged dose in the air volume. A large radial dose falloff is not expected because of the backscattering effects from the concrete walls. The dose rises in the DTL with increasing beam energy to the 10 rem/hr level, and peaks with 80 rem/hr and 60 rem/hr at the start and the end of the CCL reflecting peaks in the beam losses. The high beam losses at the start of the CCL originates from protons generated from H^--ions by double stripping processes in the DTL that are transported through the DTL and very likely lost in the first CCL tank because of the change of the RF-frequency. At the end of the CCL an excessive beam halo formation is to be expected due to a change in the transverse focusing, which drives the beam losses. The SCL has a wider aperture (see Fig. 12) and is generally equipped with a more efficient vacuum system compared to the warm linac sections, which keeps the beam losses and possible heating of the superconductiong niobium cavities at a minimum. Hence also the dose levels are comparably small there. The modulating structure of the beam loss reflected in the dose is introduced by a decrease of the aperture from 8.4 cm to 7.3 cm (see Fig. 12) in the warm sections that connect the SCL modules compared to the aperture of the cavities. Due to this design, the warm beam tube sections act as beam scrapers for the cryomodules supported by a pair of massive copper steering magnets placed in the warm sections. In the spare sections following the SCL, the quality of the vacuum dropped back to the CCL level, hence the beam loss is increased significantly to cause peak values of the dose of 200 rem/hr. The dose modulation is solely cause by particle capture and spallation reactions in the pair of copper steering magnets.

The dose levels at the very first 10 meters of DTL that is located in the front end building (see Fig. 6) range from 50 to 500 mrem/hr, as shown in Fig. 16. The doses drop only gradually to the 5 mrem/hr level 30 meters upstream of the DTL. These dose levels are caused by the high beam losses in the DTL and by back-streaming of radiation from the linac tunnel.

The dose levels are a hazard for operations personnel working in the front-end building, and need to be reduced by shields to a tolerable level of 0.25 mrem/hr. A ordinary concrete shield with a thickness of 65 cm at the start of

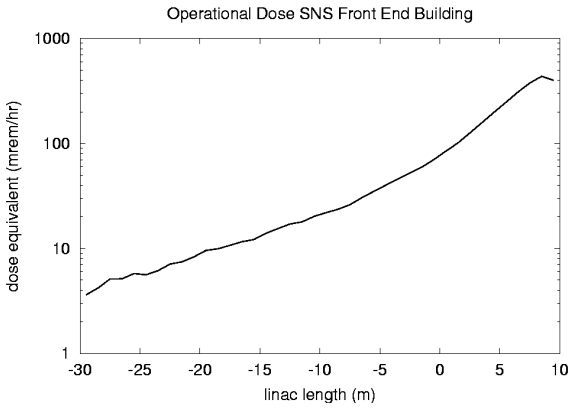

Fig. 16: Dose levels in the front-end building due to operational beam losses.

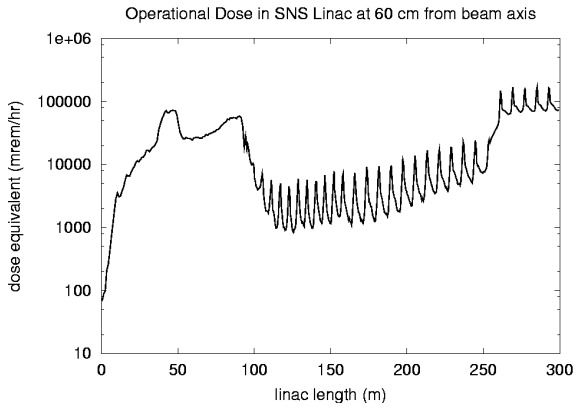

Fig. 13: Dose at 60 cm distance from the linac beam axis due to beam losses in normal operation.

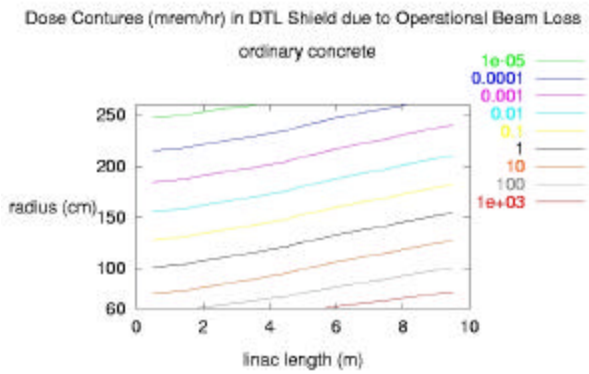

Fig. 17: Dose contours in a cylindrical ordinary concrete shield placed around the first 10 meters of the DTL.

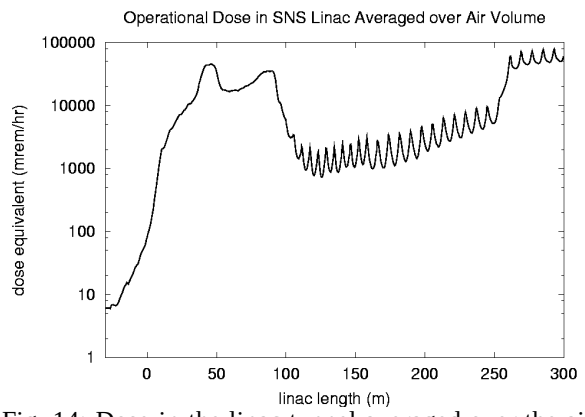

Fig. 14: Dose in the linac tunnel averaged over the air volume outside of the 60 cm radius linac envelope.

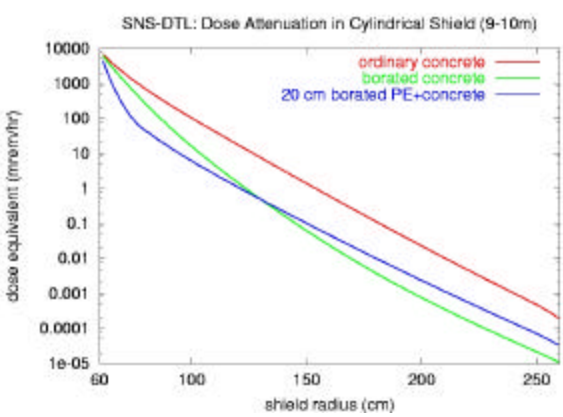

Fig. 18: Dose reduction at 9-10 meters of DTL due to cylindrical shields of various materials.

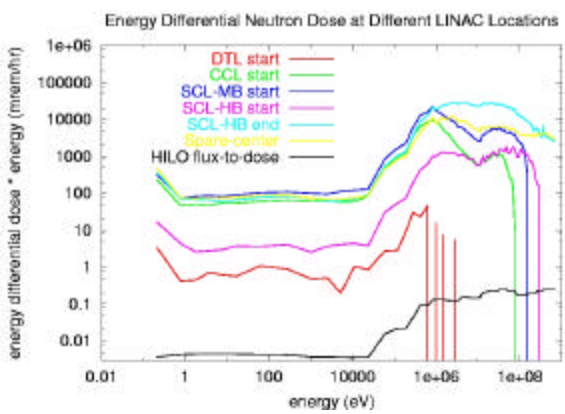

Fig. 15: Energy differential neutron doses at different linac locations, and the applied HILO flux-to-dose conversion factors in units (mrem/hr)/(n/cm^{2}s).

the DTL increasing to 120 cm at 10 meters downstream of would be required as shown in Fig. 18, if applying a cylindrical shield covering the first 10 meters of DTL. This thickness could be reduced to dimension ranging from 50 to 90 cm at the start and 10 m into the DTL, respectively, applying borated concrete (2.4 at% boron concentration), or a 20 cm thick borated polyethylene layer (2.2 at% boron concentration) followed by ordinary concrete as indicated by Fig. 19. Also a shield wall would be required to stop the radiation back-streaming from the tunnel, which needs to be looked at.

Residual dose levels of up to 5 mrem/hr were found in the DTL, 20-30 mrem/hr in the CCL, 2-5 mrem/hr in the SCL, and up to 40 mrem/hr in the spare periods following the SCL as demonstrated in Figs. 19 through 21. Thus the residual doses in the accelerator tunnel are a factor of 2000-3000 lower compared to the operational doses. For this case we assumed a 30-year operations period and a 1-hour decay period. The dose levels obtained in these fairly complex calculations are in good agreement with hand estimations performed with handbook formula from Sullivan[11], as far as those were applicable to this problem. The structure of the residual dose profiles is an image of the operational dose profiles as expected. Somewhat surprising was the fact that the activation products in the concrete of the tunnel walls contribute up to 40% of the dose for the DTL, up to 70% for the CCL, and 5-10% for the SCL and spare periods. It seems that the decay gammas from the linac structure are effectively self-shielded in the CCL because of its massive copper structures, and in the 7 cm thick stainless steel tank of the DTL.

The time development of the decay gamma power is presented in Fig. 22, which shows gamma powers relative to the shut down values for components at the end of the SCL. Whereas the gamma power of the typical stainless steel, copper and niobium structures of the linac decreases only slightly to the 90% level after one hour of decay time, the concrete already dropped to the 30% level. Even after one month of decay time the copper structures still show 50% of the initial gamma power, the steel and niobium components decreased to the 30% level and the concrete to below 10%. Not only the integral decay characteristics are of interest, but also the energy dependence of the photon spectra shown in Fig. 23 for materials discussed above. These plots reveal that in iron and copper structures the hard to shield high-energy lines above 1 MeV originate from isotopes with long decay constants, and are in significant quantities present even after 1 month of decay time. In concrete the high-energy part of the spectrum has cleared out almost completely already after one week.

VI. CONCLUSIONS

Dose profiles throughout the front-end building and the accelerator tunnel were calculated for the SNS linac system both for normal operation and after shut down of the facility based on normal operations beam losses. The calculated dose levels at an cylindrical envelope with 60 cm radius range from 0.08 to 10 rem/hr for the drift tube linac part, from 50-80 rem/hr for the coupled cavity linac part, from 1 to 20 rem/hr for the superconducting linac part, and from 70-200 rem/hr for the spare section extending after the linac. In the frontend building that houses the first 10 meters of the drift tube linac dose levels of up to 500 mrem/hr were calculated that need to be reduced by adequate shielding, for example an ordinary concrete shield of up to 120 cm thickness. The shield thickness can be reduced by 25% using borated concrete or a layer of 20 cm borated polyethylene followed by ordinary concrete. The calculated residual dose levels in the accelerator tunnel are a factor of 2000-3000 lower compared to the operational doses assuming a 30-year operations period and a 1hour decay period.

SNS is managed by UT-Battelle, LLC, under contract DE-AC00OR22725 for the U.S. Department of Energy.

VII. REFERENCES

1. National Spallation Neutron Source Conceptual Design Report, Oak Ridge National Laboratory, NSNS/CDR-2/VI, 1997.
2. SNS linac.
3. Franz X. Gallmeier, “Shielding the SNS klystron building from the linac,” Fourth International Topical Meeting on Nuclear Applications of Accelerator Technology, American Nuclear Society, Washington D.C. (November 12-15, 2000).
4. N. Catlan-Lasheras et. al., “Accelerator physics model of expected beam losses along the SNS accelerator facility during normal operation,” ANA/AP Technical Note 07, UT-Battelle, LLC, Oak Ridge (March, 2001).
5. H. G. Hughes et. al., “MCNPX for Neutron-Proton Transport,” International Conference on Mathematics & Computation, Reactor Physics & Environmental Analysis in Nuclear Applications, American Nuclear Society, Madrid, Spain, September 27-30, 1999.
6. R. G. Alsmiller jr., J. M. Barnes, and J. D. Drischler, “Neutron-photon multigroup cross sections for neutron energies less than or equal 400 MeV (Revision 1),” Oak Ridge National Laboratory, ORNL-TM 9801 (February 1986).
7. F. X. Gallmeier and P. E. Pevey, “Creation of a set of interface utilities to allow coupled Monte Carlo/discrete ordinates shielding analysis,” Third

International Topical Meeting on Nuclear Applications of Accelerator Technology, American Nuclear Society, Long Beach California, November 14-18, 1999.

8. W. W. Engle jr., "A users manual for ANISN: A one-dimensional discrete ordinates transport code with anisotropic scattering," K-1693, Oak Ridge Gaseous Diffusion Plant, Union Carbide Corp. (March 1967).
9. N. Odano et al., "Development of the Activation Analysis Calculational Methodology for the Spallation Neutron Source (SNS)," 1998 ANS radiation Protection and Shielding Division Topical Conference, American Nuclear Society, Nashville, Tennessee, April 19-23, 1998; and Greg McNeilly, "AAS-Activation Analysis System", SNS-101040200-TR0003R00, UT-Battelle (1999).
10. P. Cloth et. al., "HERMES, A Monte Carlo Program System for Beam Material Interaction Studies," KFA Juelich, Report Juel-2203 (1988).
11. A. B. Pashchenko and P. K. McLaughlin, "FENDL/A-1.1, Neutron Activation Cross Section Data Library for Fusion Applications," IAEA-NDS-148, Rev. 2 (1995).
12. A. H. Sullivan, "A Guide to Radiation and Radioactivity Levels Near Particle Accelerators," Nuclear Technology Publishing, Ashford, Kent, England, 1992.

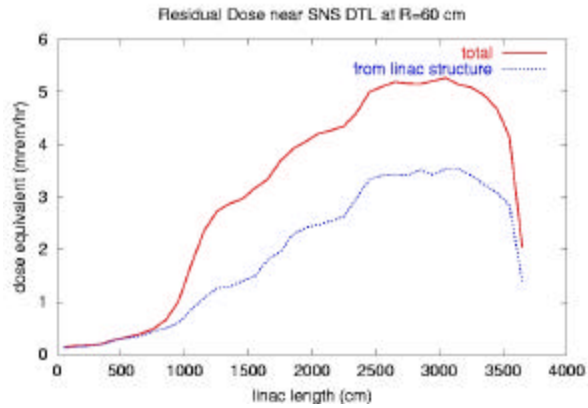

Fig. 19: Residual dose at 1 foot distance of the DTL linac after 30 year of operation and 1 hour after shut down.

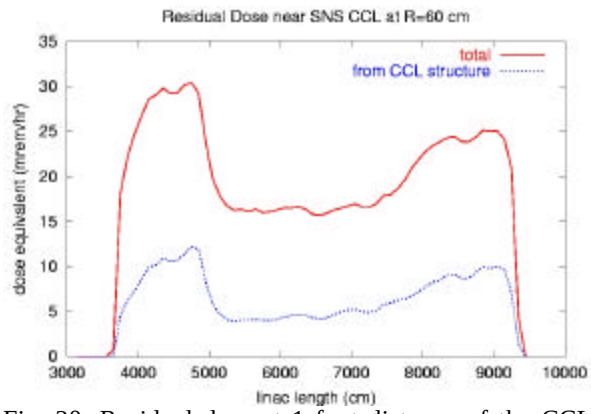

Fig. 20: Residual dose at 1 foot distance of the CCL linac after 30 year of operation and 1 hour after shut down.

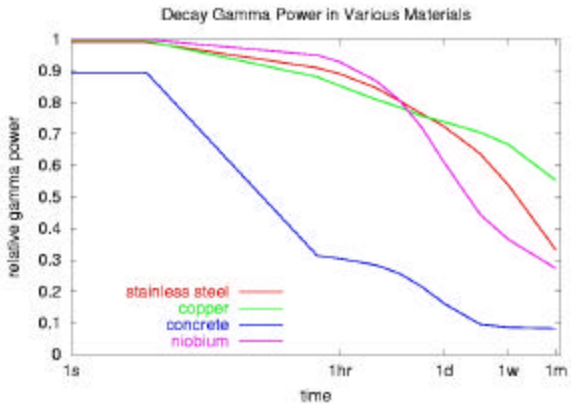

Fig. 22: Decay of the Gamma Power with time for typical components at the end of the SCL.

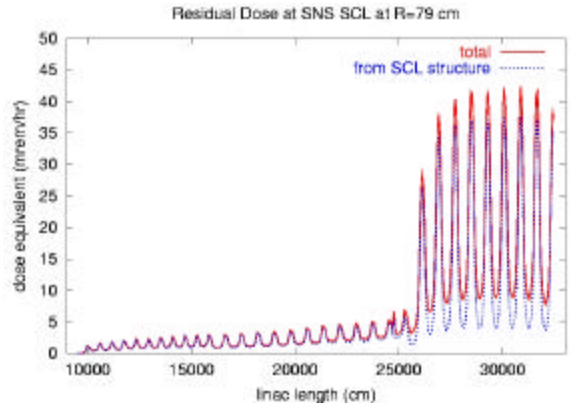

Fig. 21: Residual dose at 1 foot distance of the SCL linac and spare positions after 30 year of operation and 1 hour after shut down.

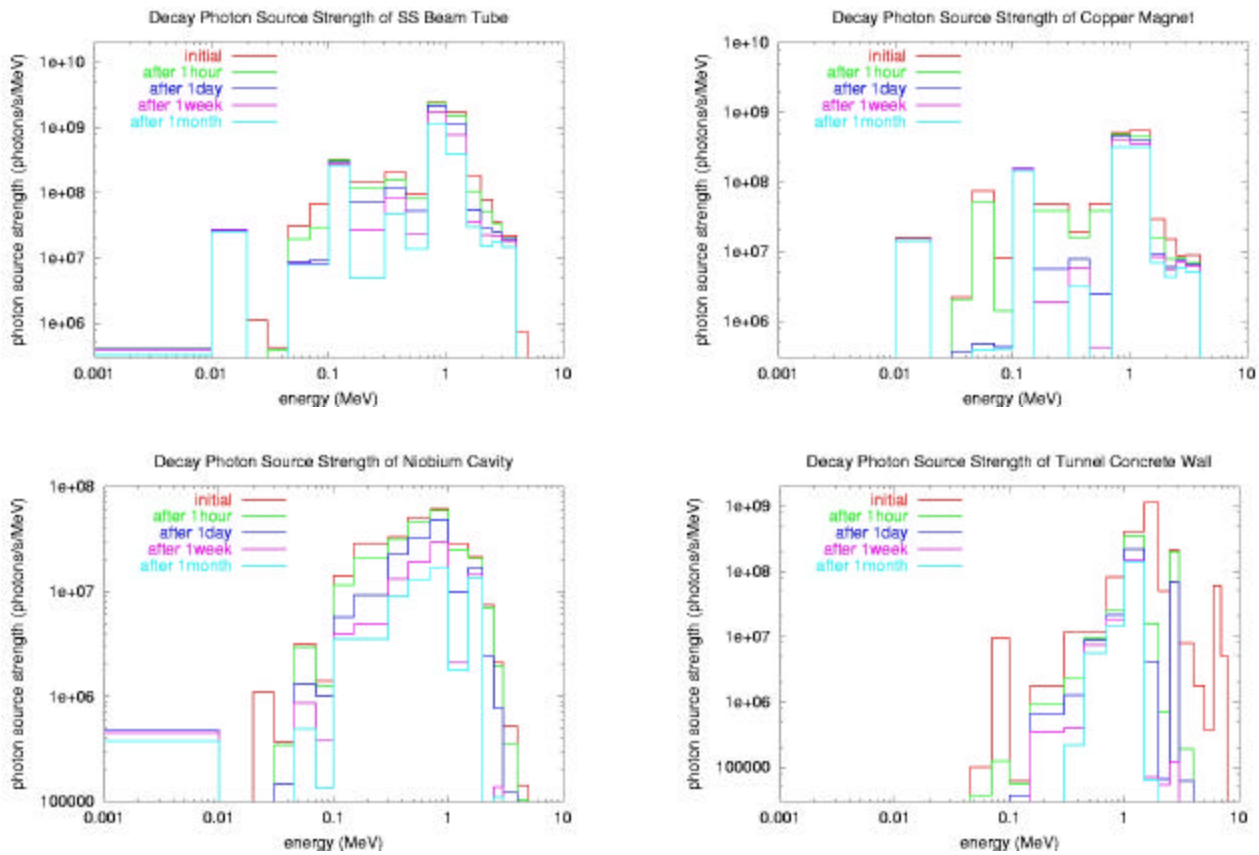

Fig. 23: Decay photon spectra for typical material zones (stainless steel, copper, niobium, and concrete) at the end of the SCL.